*Korean J. Chem. Eng.*, 38(5), 975-981 (2021)
DOI: 10.1007/s11814-021-0779-3

pISSN: 0256-1115
eISSN: 1975-7220

# N-isopropyl acrylamide/sodium acrylate hydrogel as draw agent for forward osmosis to concentrate esterification wastewater

**Yan Le*, Yanbin Yun*,†, Manxiang Wang**,†, Wenli Liu*, Shuangshuang Dong*, Kai Yang**, Syed Taj Ud Din**, Woochul Yang**, and Guicheng Liu**,†**

*College of Environmental Science and Engineering, Beijing Forestry University, Beijing 100083, P. R. China
**Department of Physics, Dongguk University, Seoul 04620, Korea
(*Received 12 December 2020 • Revised 3 March 2021 • Accepted 7 March 2021*)

**Abstract**−In recent years, a temperature-sensitive hydrogel was reported as a promising draw agent in forward osmosis (FO) technology. PEG, acts as porogen, as an enabler to improve the swelling property of hydrogels. From FO test, the addition of porogen to the hydrogel can improve the water flux of FO by increasing the swelling properties of the hydrogel. And the hydrogel modified with porogen improves the concentration efficiency of wastewater from 1.09 to 1.124 times, indicating that the modification of the hydrogel by the porogen has positive significance for FO technology. In this study, an advanced hydrogel was synthesized via physical copolymerization by using N-isopropylacrylamide and sodium acrylate. The internal structure was investigated by SEM test where it was found that that porogens have different mechanisms of action on hydrogel performance: Porogen affects the swelling property of hydrogel by changing the internal network structure through physical "occupation". The effect of porogen concentration is to act on the porosity of hydrogel, while the main effect of the molecular weight of porogen on the hydrogel structure is by altering the pore size.

Keywords: N-isopropyl Acrylamide, Thermosensitive Hydrogel, Sodium Acrylate, Forward Osmosis, Draw Agent, Porogen

## INTRODUCTION

Smart polymer hydrogel is a relatively new functional polymer material which has a three-dimensional network structure formed by a chemical bond, hydrogen bond, and van der Waals forces [1-5]. This hydrogel is water-insoluble and responsive to external stimuli (e.g., temperature, humidity, pH) due to the presence of abundant hydrophilic chemical functional groups such as hydroxyl, amide, sulfonic acid, and carboxyl [6]. Smart polymer hydrogel can be swollen or expanded up to several thousand times the dry weight of the hydrogel itself in water. The structure, physical properties, and chemical properties of the hydrogel will be changed according to the changes in the external environmental factors such as temperature, light intensity, pH, and electric field [7,8]. In particular, the temperature-sensitive hydrogel has the behavior of volume phase transition in which the volume shrinkage and expansion can be macroscopically observed with the change in temperature, hence presenting the function of water absorption and desorption. Due to its unique molecular structure, the hydrogel is widely used in agricultural field, biomedicine, and packaging industry [9-11].

Recently, there has been increasing attention to the use of the forward osmosis (FO) technology for sewage treatment. FO represents a low-energy membrane separation technology that employs osmotic pressure as a driving force [12]. The main factors thought to be influencing the performance of FO are the membrane properties and the draw agent [13,14]. However, the concentration polarization and high salt rejection possessed by the liquid agent limit the further development of FO [15].

In recent years, the temperature-sensitive hydrogel was reported as a promising draw agent in FO technology that could overcome the limitations above [16-18]. Although the hydrogel possesses the anti-salt characteristic in the FO [19], the water flux generated by the hydrogel is lower than the flux generated by the high-concentration liquid draw solution [20,21]. Therefore, increasing the water flux of temperature-sensitive hydrogels represents the common goal to the research field of FO technology. The changes of water flux can be determined by the osmotic pressure of the hydrogel considered from a few aspects, including the mixture of the polymer and water, the elastic reaction of the network, and the osmotic pressure of the ionizable molecules [19]. The most effective way is to increase the mixing ratio of the polymer and water, which in turn affects the swelling properties of the hydrogel [22]. Moreover, the contact interface between water and the hydrogel can be improved by introducing a porous layer into the hydrogel and subsequently increasing the rate of swelling and deswelling properties of the hydrogel. This method seems feasible to design a high-performance hydrogel for FO application [23].

Therefore, herein, we explored the action mechanisms of porogens on hydrogel performance, and an effective method to increase the water flux of FO through increasing the hydrogel osmotic pressure. Finally, concentrating the esterification wastewater by different hydrogels has achieved good results, which proves the positive effect of the porogen on the concentration of wastewater.

†To whom correspondence should be addressed.
E-mail: yunyanbin@bjfu.edu.cn, wmx8866@163.com, liuguicheng@dongguk.edu, log67@163.com

**Table 1. Preparation conditions for hydrogels**

| Sample No. | NIPAM (g) | SA (g) | MBA (g) | APS (g) | PEG (g) | Proportion of variable |
|---|---|---|---|---|---|---|
| 1 | 1.43 | 1.43 | 0.09 | 0.06 | 0 | PEG4000=0 wt% |
| 2 | 1.40 | 1.40 | 0.09 | 0.06 | 0.06 | PEG4000=2 wt% |
| 3 | 1.37 | 1.37 | 0.09 | 0.06 | 0.12 | PEG4000=4 wt% |
| 4 | 1.34 | 1.34 | 0.09 | 0.06 | 0.18 | PEG4000=6 wt% |
| 5 | 1.31 | 1.31 | 0.09 | 0.06 | 0.24 | PEG4000=8 wt% |
| 6 | 1.40 | 1.40 | 0.09 | 0.06 | 0.06 (PEG200) | PEG200=2 wt% |
| 7 | 1.40 | 1.40 | 0.09 | 0.06 | 0.06 (PEG400) | PEG400=2 wt% |
| 8 | 1.40 | 1.40 | 0.09 | 0.06 | 0.06 (PEG600) | PEG600=2 wt% |
| 9 | 1.40 | 1.40 | 0.09 | 0.06 | 0.06 (PEG800) | PEG800=2 wt% |
| 10 | 1.40 | 1.40 | 0.09 | 0.06 | 0.06 (PEG1000) | PEG1000=2 wt% |
| 11 | 1.40 | 1.40 | 0.09 | 0.06 | 0.06 (PEG4000) | PEG4000=2 wt% |

## EXPERIMENTAL

### 1. Hydrogel Preparation

The following steps prepared the hydrogel NIPAM/SA. Initially, the precursory materials of N-isopropyl acrylamide (NIPAM), sodium acrylate (SA), N,N-methylenebis(acrylamide) (MBA), ammonium persulfate (APS), poly(ethylene glycol) (PEG4000), and deionized water were mixed into a glass bottle and filled with nitrogen gas under the condition of 25 °C for 20 min to remove the oxygen [24-26]. Then, the glass bottle containing with all precursory materials was placed into an oscillator for 30 min. After the mixture was entirely dissolved in the glass bottle, it was sealed up to initiate the polymerization reaction at 90 °C for 2 h. The hydrogel obtained was immersed in deionized water for five days at 25 °C to remove the unreacted reagent where the deionized water was replaced every 8 h. Finally, the resulting hydrogel was placed into a vacuum oven at 70 °C for 48 h. The contents of each component are summarized in Table 1.

### 2. Preparation of FO Membrane

The FO membrane was prepared by mixing the cellulose triacetate, maleic acid, 1,4-Dioxane and acetone into a sealed Erlenmeyer flask followed by constant stirring at 25 °C for 24 h using a magnetic stirrer. Then, the obtained dissolution was degassed followed by the immersion precipitation method according to the literature to produce the FO membrane [27,28].

### 3. Measurements

3-1. FTIR Characterisation

The functional groups of hydrogel samples (NIPAM/SA and NIPAM/SA/PEG4000) and preparation materials (PEG4000, SA and NIPAM) were dried in a vacuum oven at 70 °C for 24 h and separately ground into powder. This was followed by characterization via Fourier transform infrared spectrometer (FTIR, Vertex 70, Bruker), respectively.

3-2. SEM Characterization

The morphology of hydrogel samples was determined by field emission scanning electron microscope (SEM, SU8010, Hitachi). All samples were freeze dried in vacuum freeze dryer (NAI-L1-80, Shanghai) under – 40 °C and cryogenically fractured in liquid nitrogen.

3-3. Swelling Test

The water swelling property of the hydrogel was analyzed as follows: 0.2 g of dried hydrogel was put into a dialysis bag which was then placed in 1.0 L deionized water for 24 h. The swollen hydrogel was measured after 24 h, wiped surface free water with filter paper. The swelling ratio of the hydrogels Q (g/g) was calculated by Formula 1 [29-31]:

$$Q=(W_t-W_0)/W_0 \quad (1)$$

where, $W_t$ is the weight of the hydrogel after immersion in water over a period of time, $W_0$ is the weight of the dried hydrogel, and $(W_t-W_0)$ is the weight of water absorbed by hydrogels.

3-4. Hydrogel Kinetics Test

The swelling test of the dried hydrogel was conducted by immersing the hydrogel in an excessive deionized water for 24 h, and the swelling ratio at this time was marked as equilibrium swelling ratio ($Q_e$). Before the swelling test was initiated, the weight of the dried hydrogel was recorded. Then, the hydrogel was immersed in the deionized water in which the weight of the hydrogel was recorded every 30 min throughout the test. The free water presence on the surface of the hydrogel was wiped with filter paper before every measurement, and the swelling ratio at different time was marked as instantaneous swelling ratio ($Q_t$). The water absorption ratio can be calculated by Formula 1.

An efficient integration formula for the swelling kinetics was deduced directly from the swelling ratio, Formula 2:

$$kt=In[(Q_e-Q_0)/(Q_e-Q_t)] \quad (2)$$

where, $Q_e$ is equilibrium swelling ratio, $Q_0$ is initial swelling ratio of the dried hydrogel, and $Q_t$ is instantaneous swelling ratio.

The swelling kinetics was analyzed by plotting the graph of $In[(Q_e-Q_0)/(Q_e-Q_t)]$ versus time t, and the slope of the curve k refers to swelling rate.

3-5. FO Measurement

FO measurements were carried out in homemade equipment, schematically illustrated in Fig. 1. 0.2 g of dry hydrogel was immersed in deionized water for five minutes to activate the hydrogel ions, and then the hydrogel was placed on the active side of the FO membrane as a draw agent while different concentration of the solution or deionized water was placed on the other side. The water flux, F (LMH), was calculated using Formula 3 [32]:

$$F=V/(A\times T) \quad (3)$$

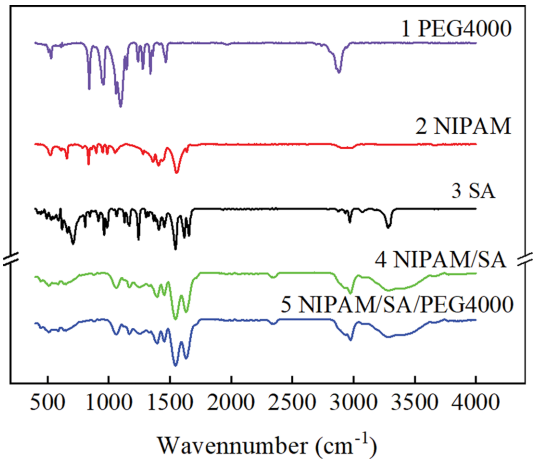


**Fig. 1. FTIR of PEG4000, SA, NIPAM, NIPAM/SA, and NIPAM/SA/PEG4000.**

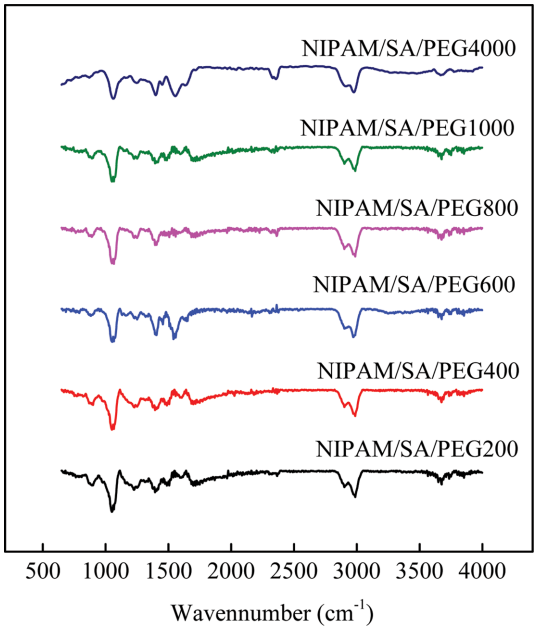


**Fig. 2. FTIR of hydrogels with different molecular weight of PEG.**

where, V (L) is the volume of water absorbed by the hydrogel via the FO membrane, calculated by dividing the mass of the water by its density. Here, the mass of water was measured by an analytical balance (BSM-120.4, Shanghai). A ($m^2$) is the effective area of FO membrane ($6\times10^{-4}$ $m^2$), and T (h) is the process time of the test.

3-6. Concentrating Test

Using NIPAM/SA and NIPAM/SA/PEG4000 as draw agents, respectively, esterified wastewater (COD=500 ppm) was tested by the above method of FO measurement for 12 hours. The water flux and COD concentration of the raw material solution were recorded each hour in the process.

## RESULTS AND DISCUSSION

### 1. FTIR Spectrum Analysis of Hydrogels

The occurrence of polymerization was confirmed by FTIR of the final solid material (PEG4000, SA, NIPAM) and hydrogel powder, as shown in Fig. 1. The curves of 1, 2, 3, 4, and 5 on Fig. 1 represent the FTIR spectrum of PEG4000, SA, NIPAM, NIPAM/SA, and NIPAM/SA/PEG4000, respectively. Comparing the curves 4, 5 with 2 and 3, the presence of hydrogel-specific hydrophobic functional group (-CH($CH_3$)) at 1,398 $cm^{-1}$ and 1,452 $cm^{-1}$, the hydrophilic functional group (-$CONH_2$) at 1,542 $cm^{-1}$, N-H bending and C-H bending at 3,400 $cm^{-1}$ and 2,975 $cm^{-1}$, respectively, strongly indicate the successful synthesis of the hydrogel (NIPAM/SA/PEG4000) by physical co-polymerization. Adsorption bands at 1,100 $cm^{-1}$ related with the C-OH groups in unreacted PEG 4000 (curve 1), are absent in the final copolymer (curve 4, 5), which represents PEG 4000 as an additive does not participate in hydrogel polymerization.

The curves in Fig. 2 show the similar vibrational absorption peak of hydrogel-specific groups. It proved that the hydrogels have been successfully synthesized, and the different molecular weight of PEG did not alter the chemical groups of hydrogel.

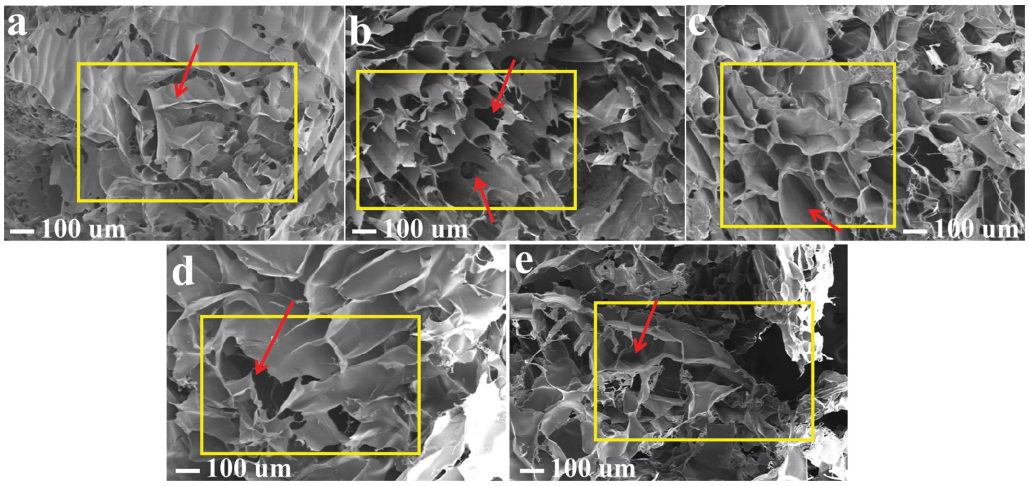


**Fig. 3. SEM images of hydrogel samples. (a) NIPAM/SA, (b) NIPAM/SA/2 wt%PEG4000, (c) NIPAM/SA/4 wt%PEG4000, (d) NIPAM/SA/6 wt%PEG4000, and (e) NIPAM/SA/8 wt%PEG4000.**

## 2. Morphologies of Hydrogels

Fig. 3 shows SEM images of cross-sections of freeze-dried hydrogel samples. It can be seen that all samples have well-defined porous structure. But there is a difference in the size and number of pores with different amount of PEG4000 participating in the phase separation process. The surface morphology of the irregular pores was observed in the SEM image of NIPAM/SA not modified by PEG4000, while the network structure formed was not obvious (Fig. 3a). By the addition of the porogen, the surface of the NIPAM/SA/PEG4000 exhibits a regular porous microscopic network structure (Fig. 3b). The addition of PEG4000 in polymer reaction phase endows the hydrogel with pores, and the internal network structure of hydrogel becomes more regular with increasing amount of PEG4000 from 2 wt% to 4 wt% (Fig. 3b, 3c). The formation of the regular porous structure can be explained as that PEG4000 provides a space barrier in the hydrogel network at initial polymerization stage, and then pores result produced after phase separation of the homogeneous polymer solution. As the PEG4000 content continues to increase from 4 wt% to 8 wt%, the network structure becomes irregular, mainly because excessive PEG4000 presents a more interconnected pore structure to destroy the uniform porous structure (Figs. 3c-3e).

SEM images of the internal network structure of hydrogels with varying molecular weight of PEG are exhibited in Fig. 4. It can be seen from the cross-sections of hydrogels, as the molecular weight increases from 200 to 4,000, the difference of internal structures is more obvious that the size of the pores is interestingly larger, and the network structure becomes more regular.

## 3. Swelling and Deswelling Properties of Hydrogels

The swelling ratio of hydrogel samples with varying content of PEG4000 as a function of swelling time is plotted in Fig. 5(a). It can be seen that in the preliminary stage, all the hydrogel samples rapidly absorbed water, and the swelling ratio obviously increased over time. As the content of PEG4000 increased from 0 wt% to 2 wt%, the water absorption rate and the equilibrium swelling rate were interestingly improved from 138.43 g/g to 167.83 g/g. However, with the content of PEG4000 continuing to increase from 2 wt% to 8 wt%, the water absorption rate and equilibrium swelling rate declined from 167.83 g/g to 103.25 g/g, indicating that excess content of PEG4000 could restrain the water absorption capacity of the hy-

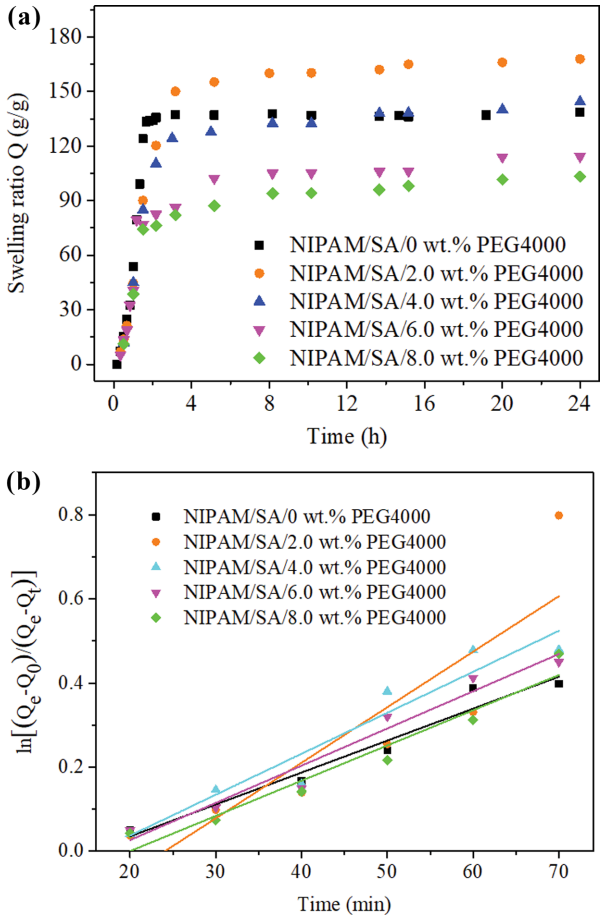


**Fig. 5. (a) Swelling ratio of NIPAM/SA/PEG4000 hydrogels with varying content of PEG4000. (b) Hydrogel kinetics of NIPAM/SA/PEG4000 hydrogels with varying content of PEG4000.**

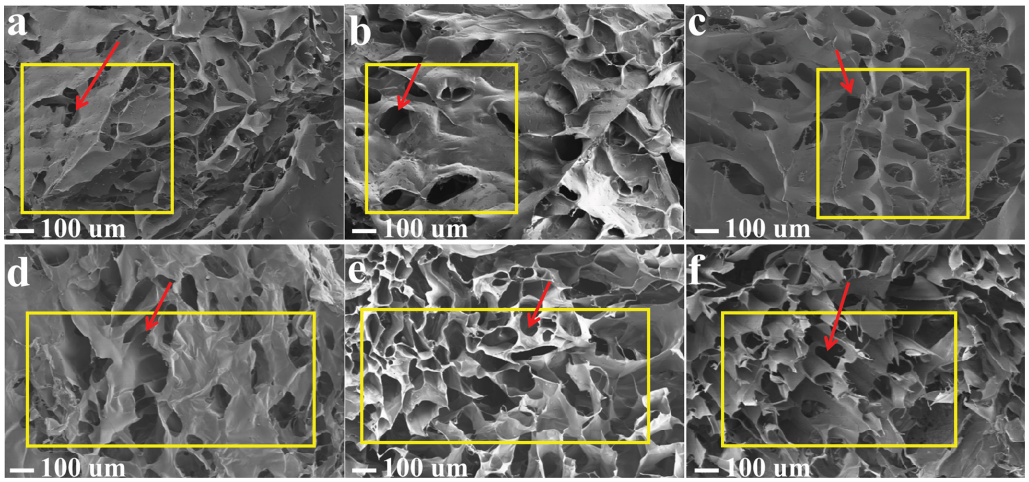


**Fig. 4. SEM images of hydrogel samples. (a) NIPAM/SA/PEG200, (b) NIPAM/SA/PEG400, (c) NIPAM/SA/PEG600, (d) NIPAM/SA/PEG800, (e) NIPAM/SA/PEG1000, (f) NIPAM/SA/PEG4000.**

**Table 2. Swelling rate constant of NIPAM/SA hydrogel and NIPAM/SA/PEG4000 hydrogels with varying content of PEG**

| Samples | Swelling rate constant k ($10^{-3}$ $h^{-1}$) | Adj.R-square (%) |
|---|---|---|
| NIPAM/SA/0 wt% PEG4000 | 7.6 | 95.43 |
| NIPAM/SA/2 wt% PEG4000 | 13.2 | 94.16 |
| NIPAM/SA/4 wt% PEG4000 | 9.7 | 98.21 |
| NIPAM/SA/6 wt% PEG4000 | 8.8 | 95.01 |
| NIPAM/SA/8 wt% PEG4000 | 8.4 | 93.38 |

drogels. This conclusion is consistent with the above experimental results of SEM section: appropriate amount of porogens could improve the performance of hydrogel by promoting the network pore size and the more uniform network structure, while the excess amount of porogen would reduce capillary action on account of over-dense interpenetrating porous structure.

By plotting the graph of $\ln[(Q_e-Q_0)/(Q_e-Q_t)]$ versus time t of hydrogel samples with varying content of PEG4000 and linearly fitting the curves of graph, as is shown in Fig. 5(b), the swelling rate constant k was obtained from slopes of fitting graphics, which are listed in Table 2. To justify the slope-decreasing along with the PEG-content increasing, the swelling rate of the hydrogel added with 2 wt% PEG4000 increased by 21.24%, while the k value rose by 73.68% than the original one, which means the swelling rate has been increased. As seen in Fig. 5 and Table 2, the NIPAM/SA/PEG4000 hydrogel with PEG-porogen added has a higher swelling rate than that of NIPAM/SA without being modified by pore former, indicating that PEG4000, as a porogen, has an improved performance on the hydrogel. Because, large pores provide enough space for hydrophilic group-contact-points with water molecules, thereby accelerating the water absorption rate. Whereas, NIPAM/SA/2 wt%PEG4000 shows highest swelling rate, demonstrating an excess of the porogen would restrain the hydrogel offering its best performance on pore-forming.

The swelling ratio of hydrogel samples with varying molecular weight of PEG as a function of swelling time is shown in Fig. 6(a). It can be seen that as the molecular weight of PEG increases from 200 to 4,000, the equilibrium swelling ratio of the hydrogel is improved from 140.1 g/g to 167.83 g/g, rising by 19.8%, implying that, the molecular weight of PEG has a positive promotion effect on water absorption properties of hydrogel in the test range.

Fig. 6(b) is the curve of ln $[(Q_e-Q_0)/(Q_e-Q_t)]$ versus time t of hydrogel samples with varying molecular weight of PEG. The swelling rate constant k was obtained by linearly fitting the curves, which are listed in Table 3. It can be seen that with the molecular weight of PEG increasing, the swelling rate increases slightly, illustrating porogens improve the performance of hydrogels, to some extent, and the contribution of high molecular weight is more visible.

From the above conclusion of the SEM test, the size of hydrogel pores would increase as the molecular weight of the PEG inbcreased. Therefore, the water absorption rate and retention properties of the hydrogel are improved with the molecular weight of PEG increased.

## 4. FO Testing with Esterification Wastewater

From the above swelling ratio experiment, it can be concluded

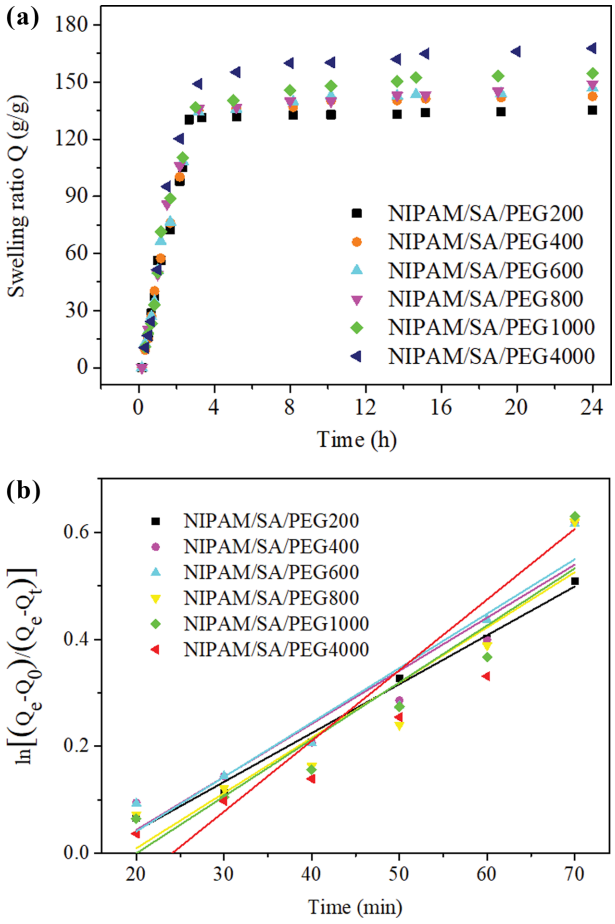


**Fig. 6. (a) Swelling ratio of NIPAM/SA hydrogels with varying molecular weights. (b) Hydrogel kinetics of NIPAM/SA hydrogels with varying molecular weights.**

**Table 3. Swelling rate constant of NIPAM/SA hydrogels with varying molecular weight of PEG**

| Samples | Swelling rate constant k ($10^{-3}$ $h^{-1}$) | Adj.R-square (%) |
|---|---|---|
| NIPAM/SA/PEG200 | 9.1 | 98.63 |
| NIPAM/SA/PEG400 | 9.9 | 89.89 |
| NIPAM/SA/PEG600 | 10.2 | 91.21 |
| NIPAM/SA/PEG800 | 10.3 | 86.24 |
| NIPAM/SA/PEG1000 | 10.6 | 87.23 |
| NIPAM/SA/PEG4000 | 13.2 | 74.35 |

that all the hydrogel samples basically reached swelling equilibrium in 3 h; therefore, 3 h was chosen as the test time for the FO water flux test. To investigate the effect of hydrogel porogens on FO technology, NIPAM/SA/2.0 wt%PEG4000 hydrogel and NIPAM/SA were chosen as draw agents.

In Fig. 7, water fluxes in the 3 h FO process using NIPAM/SA hydrogels and NIPAM/SA/PEG4000 hydrogels as draw agents, deionized water and varying concentration of esterification wastewater (COD concentration=1,000 ppm, 2,000 ppm, 4,000 ppm, 6,000 ppm, 8,000 ppm) as the feed solution are shown, respectively. Fig. 7 shows

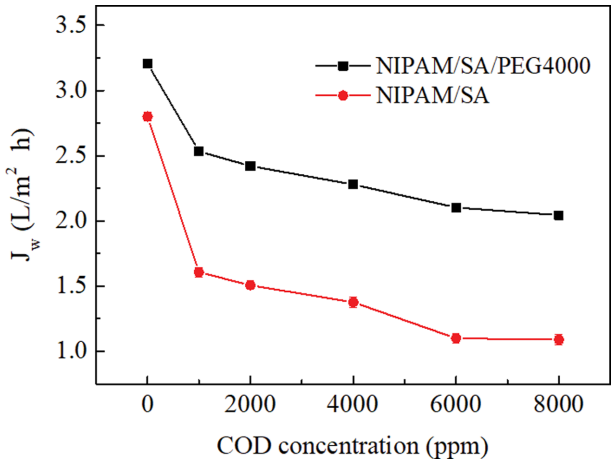


**Fig. 7. Effect of porogen on water flux.**

the FO water flux of pure hydrogel and porogen modified hydrogel in deionized water and esterified wastewater with varying concentrations of COD (COD concentration=1,000 ppm, 2,000 ppm, 4,000 ppm, 6,000 ppm, 8,000 ppm) When pure water was used as feed solution, NIPAM/SA/PEG4000 and NIPAM/SA generated 4.62 LMH and 3.91 LMH FO water flux, respectively. And when 1,000 ppm esterified wastewater was used as feed solution, the water flux of NIPAM/SA/PEG4000 dropped significantly with decreased by 15.37%, because, it is well known that, high concentration of COD leads to the reduction of osmotic pressure. Even so, it is still higher than that of NIPAM/SA with decreasing by 30.14%. As the concentration of esterification wastewater increased from 2,000 ppm to 8,000 ppm, the FO water flux produced by the two hydrogels showed a similar trend. But the decline degree of NIPAM/SA (decreased by 16.44%) is larger than that of NIPAM/SA/PEG4000 (decreased by 13.33%), indicating that the porogen promotes the progress of the FO process by enhancing the driving force of draw agents. This proves that the porogen had enhanced the water absorption properties of hydrogel and meanwhile also enhanced the osmotic pressure of the forward osmosis that subsequently improved the forward osmosis process. And as observed from the changes of the COD concentrations, the water flux produced by the modified hydrogel was smaller than that of the unmodified hydrogel. This proves that the hydrogel modified by porogens can optimize the application of hydrogel as an extractant in the FO process.

The result of the concentration test on esterification wastewater by FO technology is shown in Fig. 8. Over time, the concentration of esterification wastewater increased, from the original 500 ppm to 545 ppm and 562 ppm, respectively, which is 1.09 times and 1.124 times. It is proved that the hydrogels can be used to concentrate part of the wastewater through FO technology, which is valuable in terms of concentration. In addition, the water flux produced by NIAPM/SA/PEG4000 is greater than that of NIPAM/SA, which has an obvious advantage on concentration. Therefore, porogen can enhance the adaptability value of hydrogel draw agent in FO technology.

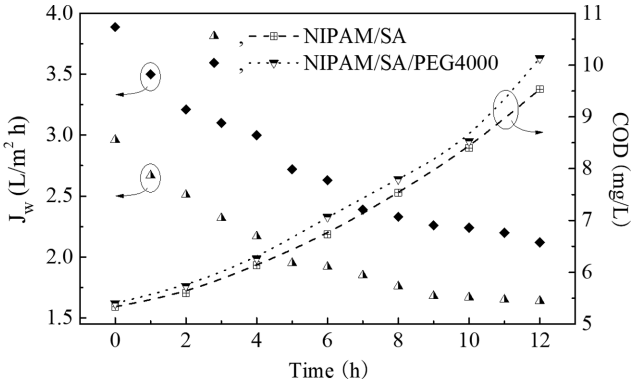


**Fig. 8. Water flux and COD concentration of NIPAM/SA and NIPAM/SA/PEG4000 under the FO mode.**

## CONCLUSIONS

This paper presents that the addition of porogen to hydrogel can improve the water flux of FO by increasing the swelling properties of the hydrogel. This paper presents that porogens have different mechanisms of action on hydrogel performance, and the addition of porogen to the hydrogel can improve the water flux of FO by increasing the swelling properties of the hydrogel. Porogen affects the swelling property of hydrogel by changing the internal network structure through physical "occupation". The effect of porogen concentration is to act on porosity of hydrogel, while the main effect of the molecular weight of porogen on the hydrogel structure is by altering the pore size. The concentration test shows that both NIPAM/SA/PEG4000 and NIPAM/SA hydrogels can concentrate wastewater with a certain concentration and have certain application value. Among them, the water flux and concentrated effect produced by NIPAM/SA/PEG4000 were better than that of NIPAM/SA; the COD concentration of wastewater is concentrated by 1.124 times and 1.09 times, respectively. Therefore, the porogen can improve the positive osmosis efficiency by improving the swelling property, which demonstrates that the hydrogel modified by porogen (NIPAM/SA/PEG4000) shows promise to be used as a draw agent in forward osmosis technology.

## ACKNOWLEDGEMENTS

This work was supported by the National Key Research and Development Program of China (No. 2018YFB0604302-03), the Brain Pool program funded by the Ministry of Science and ICT through the National Research Foundation of Korea (No. 2019H1D3A2A02100593), and the National Research Foundation of Korea (NRF) grant funded by the Korean government (MSIT) (Nos. 2019R1C1C1006310, 2020R1I1A1A01072996, and 2019R1A2C1002844).

## SUPPORTING INFORMATION

Additional information as noted in the text. This information is available via the Internet at http://www.springer.com/chemistry/journal/11814.

## REFERENCES


1. N. Eslahi, M. Abdorahim and A. Simchi, *Biomacromolecules*, **17**(11), 3441 (2016).
2. M. Li, H. Wang, J. Hu, J. Hu, S. Zhang, Z. Yang, Y. Li and Y. Cheng, *Chem. Mater.*, **31**(18), 7678 (2019).
3. X. Li and X. Su, *J. Mater. Chem. B*, **6**, 4714 (2018).
4. Y. Wang, C. Dong, D. Zhang, P. Ren, L. Li and X. Li, *Int. J. Min. Met. Mater.*, **22**, 998 (2015).
5. R. James and C. T. Laurencin, *Rare Metals*, **34**, 143 (2015).
6. J. J. Duan and L. N. Zhang, *Chin. J. Polym. Sci.*, **35**, 1165 (2017).
7. J. M. Corpart and F. Candau, *Macromolecules*, **26**, 1333 (1993).
8. T. Begam, A. K. Nagpal and R. Singhal, *J. Appl. Polym. Sci.*, **89**, 779 (2003).
9. X. Li, Q. Li, X. Xu, Y. Su, Q. Yue and B. Gao, *J. Taiwan Inst. Chem. E.*, **60**, 564 (2016).
10. Y. K. Lin, R. Sharma, H. Ma, W. S. Chen and C. L. Yao, *J. Taiwan Inst. Chem. E.*, **20**, 1 (2017).
11. C. Fuciños, P. Fuciños, M. Míguez, I. Katime, L. M. Pastrana and M. L. Rúa, *Plos One*, **9**, e87190 (2014).
12. W. Wang, Y. Guo, M. Liu, X. Song and J. Duan, *Korean J. Chem. Eng.*, **37**, 1573 (2020).
13. Q. Yang, J. Lei, D. D. Sun and D. Chen, *Sep. Purif. Rev.*, **45**, 93 (2016).
14. L. Chekli, S. Phuntsho, H. K. Shon, S. Vigneswaran, J. Kandasamy and A. Chanan, *Desalin. Water Treat.*, **43**, 167 (2012).
15. S. Mansouri, S. Khalili, M. Peyravi, M. Jahanshahi, R. R. Darabi, F. Ardeshiri and A. S. Rad, *Korean J. Chem. Eng.*, **35**, 2256 (2018).
16. D. Li, X. Zhang, J. Yao, G. P. Simon and H. Wang, *Chem. Commun.*, **47**, 1710 (2011).
17. R. Ou, Y. Wang, H. Wang and T. Xu, *Desalination*, **318**, 48 (2013).
18. Q. Ge, J. Su, G. L. Amy and T. S. Chung, *Water Res.*, **46**, 1318 (2012).
19. D. Li and H. Wang, *J. Mater. Chem. A*, **1**, 14049 (2013).
20. A. Shakeri, M. T. Nakhjiri, H. Salehi, F. Ghorbani and N. Khankeshipour, *J. Water Process Eng.*, **24**, 42 (2018).
21. Y. Cai, W. Shen, S. L. Loo, W. B. Krantz, R. Wang, A. G. Fane and X. Hu, *Water Res.*, **47**, 3773 (2013).
22. K. Kabiri and M. J. Zohuriaan-Mehr, *Macromol. Mater. Eng.*, **289**, 653 (2004).
23. D. Li, X. Zhang, J. Yao, Y. Zeng, G. P. Simon and H. Wang, *Soft Matter*, **7**, 10048 (2011).
24. S. Sun and P. Wu, *Macromolecules*, **43**, 9501 (2010).
25. F. Kousar, M. A. Malana, A. H. Chughtai and M. S. Khan, *Polym. Bull.*, **75**, 1275 (2018).
26. A. K. Saikia, S. Aggarwal and U. K. Mandal, *J. Polym. Res.*, **20**, 1 (2013).
27. T. P. N. Nguyen, E. T. Yun, I. C. Kim and Y. N. Kwon, *J. Membr. Sci.*, **433**, 49 (2013).
28. G. Li, X. M. Li, T. He, B. Jiang and C. J. Gao, *Desalin. Water Treat.*, **51**, 2656 (2013).
29. S. Dong, Y. Yun, M. Wang, C. Li, H. Fu, X. Li, W. Yang and G. Liu, *J. Taiwan Inst. Chem. E.*, **117**, 56 (2021).
30. B. Li, Y. Yun, M. Wang, C. Li, W. Yang, J. Li and G. Liu, *Desalination*, **500**, 114889 (2021).
31. Y. Bao, J. Z. Ma and N. Li, *Carbohyd. Polym.*, **84**, 76 (2011).
32. Y. Zeng, Q. Ling, K. Wang, J. F. Yao, D. Li, G. P. Simon, R. Wang and H. Wang, *RSC Adv.*, **3**, 887 (2013).

# Supporting Information

# N-isopropyl acrylamide/sodium acrylate hydrogel as draw agent for forward osmosis to concentrate esterification wastewater

**Yan Le*, Yanbin Yun*,†, Manxiang Wang**,†, Wenli Liu*, Shuangshuang Dong*, Kai Yang**, Syed Taj Ud Din**, Woochul Yang**, and Guicheng Liu**,†**

*College of Environmental Science and Engineering, Beijing Forestry University, Beijing 100083, P. R. China
**Department of Physics, Dongguk University, Seoul 04620, Korea
(*Received 12 December 2020 • Revised 3 March 2021 • Accepted 7 March 2021*)

**Note:**

*Materials:* N-isopropyl acrylamide (NIPAM, 98%) and sodium acrylate (SA, 95%) were purchased from Xiya Chemical Industry and Tianjin Heowns Biochem Industry, respectively. The N,N-methylenebis(acrylamide) (MBA, 99%) and ammonium persulfate (APS, 98%) were obtained from Shanghai Chemical Industry. The FO membrane tested in this study was produced using several materials, including cellulose triacetate (CTA) (Eastman Chemical Company), maleic acid (95%) (Shanghai Yuanye Biotechnology Industry), acetone (95%) and 1,4-Dioxane (99%) (Beijing Chemical Works). Pure water used in all experiments was obtained by Lanyi Company.

**Table S1. Ra points of AHC, TS-AHC, and modified TN-AHC-P membranes**

| Membrane | AHC | TS-AHC | TN-AHC-P |
|---|---|---|---|
| Ra point (nm) | 66.9 | 46.5 | 75.2 |

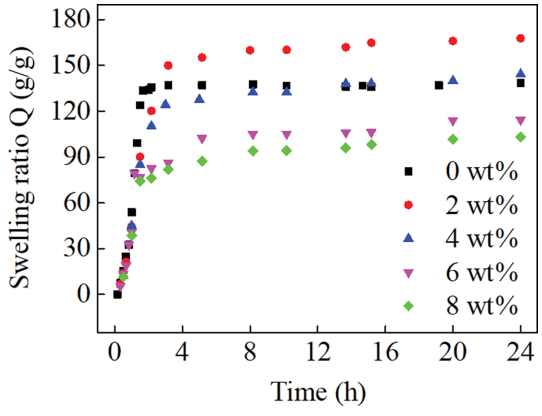


**Fig. S1. Swelling ratio of NIPAM/SA/PEG4000 hydrogels with varying content of PEG4000.**

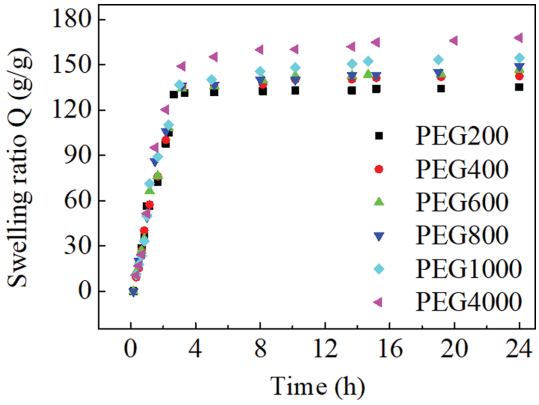


**Fig. S2. Swelling ratio of NIPAM/SA hydrogels with varying molecular weights.**

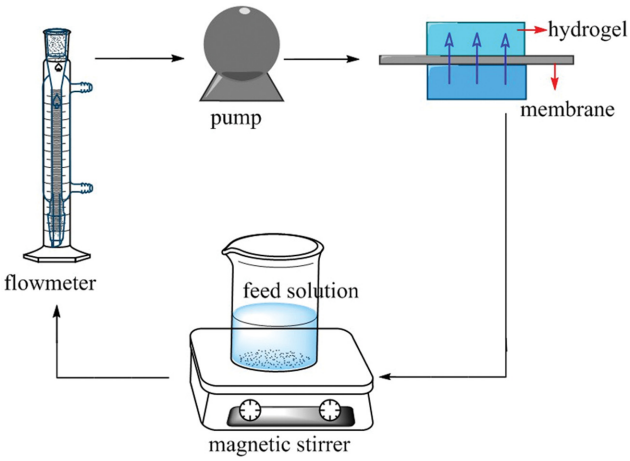


**Fig. S3. Schematic diagram of forward osmosis test.**